ADVANCED FUNCTIONAL MATERIALS
www.afm-journal.de



# Gradual Controlling the Work Function of Metal Electrodes by Solution-Processed Mixed Interlayers for Ambipolar Polymer Field-Effect Transistors and Circuits

*Dang Xuan Long, Kang-Jun Baeg, Yong Xu, Seok-Ju Kang, Myung-Gil Kim, Geon-Woong Lee, and Yong-Young Noh**

**In this paper, a technique using mixed transition-metal oxides as contact interlayers to modulate both the electron- and hole-injections in ambipolar organic field-effect transistors (OFETs) is presented. The cesium carbonate ($Cs_2CO_3$) and vanadium pentoxide ($V_2O_5$) are found to greatly and independently improve the charge injection properties for electrons and holes in the ambipolar OFETs using organic semiconductor of diketopyrrolopyrrolethieno[3,2-b]thiophene copolymer (DPPT-TT) and contact electrodes of molybdenum (Mo). When $Cs_2CO_3$ and $V_2O_5$ are blended at various mixing ratios, they are observed to very finely and constantly regulate the Mo's work function from −4.2 eV to −4.8 eV, leading to high electron- and hole-mobilities as high as 2.6 and 2.98 $cm^2 V^{-1} s^{-1}$, respectively. The most remarkable finding is that the device characteristics and device performance can be gradually controlled by adjusting the composition of mixed-oxide interlayers, which is highly desired for such applications as complementary circuitry that requires well matched n-channel and p-channel device operations. Therefore, such simple interface engineering in conjunction with utilization of ambipolar semiconductors can truly enable the promising low-cost and soft organic electronics for extensive applications.**

## 1. Introduction

Conjugated organic molecules are emerging as materials for use as active layers in soft electronics.[1–3] Their soft mechanical properties natively enable flexible, even stretchable, electronic and optoelectronic devices, such as for displays,[4–7] photovoltaics,[8] sensors,[9] memory drives,[10,11] and microprocessors.[12] After functionalization with side chains, the solution-processed organic semiconductors can change a paradigm for the manufacture of electronic devices by replacing the conventional photolithography and high vacuum-based processes via a variety of high-throughput, cost-effective graphic art printing techniques.[13] Organic field-effect transistors (OFETs) are one of the most important building blocks of soft electronic circuits, and they provide a basis for understanding the charge transport mechanism in organic semiconductors and those in other organic devices.[14] Moreover, the multi-functionalization of OFETs could greatly broaden their applicability to novel devices such as flash memory,[15,16] photo/chemical-sensors,[17] and light-emitting transistors.[18] In most cases, their functionalities are derived from (and/or are enhanced by) the contribution of both electron and hole transport, which is ambipolar in nature, to realize ambipolar OFETs. These devices necessitate efficient and balanced charge injection/extraction for electrons and holes simultaneously.

Complementary metal-oxide semiconductor (CMOS)-like electronic circuits, with which a facile fabrication route to compose cheaper printed organic microprocessors compared to the present silicon technology can be naturally delivered, are another fascinating application of ambipolar OFETs.[19] Conventional silicon CMOS circuits consist of individual *n*-type and *p*-type transistors fabricated with different doping and designed to have equivalent output currents. However, for building organic CMOS circuits, unipolar *n*-type and *p*-type organic semiconductors with comparable electronic properties generally need to be developed first, and the resulting fabrication processes for the two different semiconductors become sophisticated. A promising alternative is to use ambipolar OFETs with only a single layer of ambipolar semiconductor that serves as both the *n*-type and *p*-type transporting mediums. In this way, a much-simplified fabrication process for low-cost and large-area electronics can be easily achieved. The printable ambipolar OFETs were typically achieved by using a single component[20–22] or by

D. X. Long, Prof. Y. Xu, Dr. S.-J. Kang, Prof. Y.-Y. Noh
Department of Energy and Materials Engineering
Dongguk University
26 Pil-dong, 3-ga, Jung-gu,
Seoul 100–715, Republic of Korea
E-mail: yynoh@dongguk.edu
Dr. K.-J. Baeg, Dr. G.-W. Lee
Nanocarbon Materials Research Group
Korea Electrotechnology Research Institute (KERI)
12 Bulmosan-ro 10beon-gil, Seongsan-gu, Changwon
Gyeongsangnam-do 642–120, Republic of Korea
Prof. M.-G. Kim
Department of Chemistry
Chung-Ang University
84 Heukseok-ro, Dongjak-gu, Seoul, Republic of Korea

DOI: 10.1002/adfm.201401154

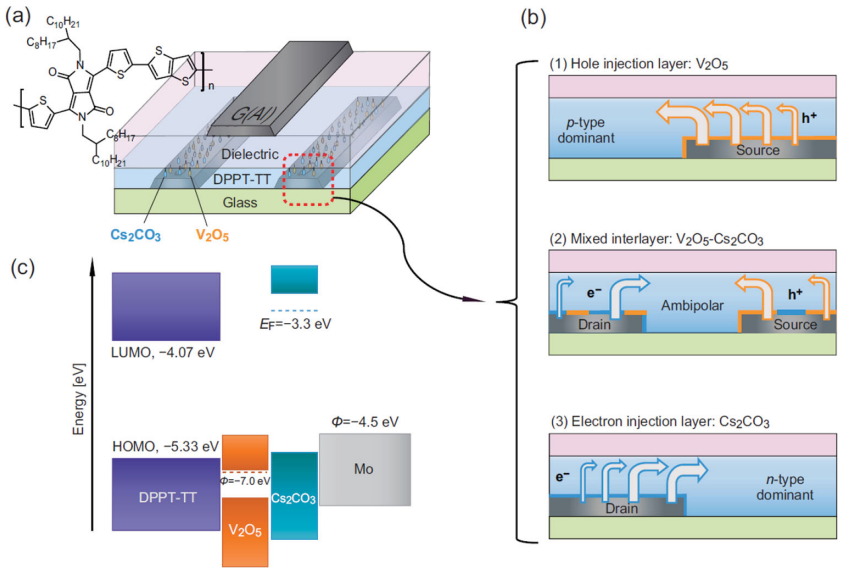


**Figure 1.** a) Chemical structure of the DPPT-TT ambipolar semiconductor and TG/BC OFET device structure. b) Schematic illustration of hole- and electron-injection through the interlayer of ambipolar OFETs, and c) energy band diagram of the charge injection from various interlayer-incorporated Mo electrodes.

blending of individual *p*-type and *n*-type organic semiconductors (soluble small molecules or polymers).[23–25]

To ensure high-performance CMOS-like organic circuits, ambipolar organic semiconductors should have similarly high electron and hole mobility as well as a small threshold voltage ($V_{Th}$) for *n*- and *p*-channel operations. The state-of-the-art $\pi$-conjugated polymer semiconductors, especially those with a donor–acceptor copolymer structure, have shown impressive progress with high mobility (i.e., more than 1.0 $cm^2\ V^{-1}\ s^{-1}$ for both *n*- and *p*-channel operations).[19] The high carrier mobility in those ambipolar OFETs is mainly attributable to the strong inter-chain interaction between polymer backbones with push–pull electronic structures, and optimized device configuration that prevents the mobile charge from being trapped and facilitates efficient charge injections from common source/drain electrodes to a polymer semiconductor. In a system with smaller band-gap semiconductor, the injection barrier to the electrons and the holes can be decreased concomitantly. However, this still leads to an unfavorable charge–injection barrier for one type of charge carrier unless a zero band-gap semiconductor, such as graphene, is used.

Consequently, Ohmic contacts for both electrons and holes by contact engineering on common metal electrodes become a crucial issue. In fact, several approaches to contact resistance ($R_c$) reduction have been reported,[26] such as interfacial doping in the vicinity of contacts, the introduction of injection interlayers, and the deposition of self-assembled monolayers (SAMs) on metal electrodes. Although these approaches have successfully modified the work function ($\Phi$) of metal electrodes for lowering the charge-injection barrier, they are only effective for one type of charge carrier, either electrons or holes. Because electron-injection and hole-injection share the same contacts and a constant band gap, reducing the energy barrier for one type of charge carrier will inevitably increase the barrier height for the other. A novel methodology is thus highly desirable to simultaneously improve electron and hole injection and to systematically control the charge injection for adjusting the *n*- and *p*-channel behaviors of ambipolar devices.

Here, we report on the gradual control of the metal electrode's work function ($\Phi$) by incorporating a solution-processed mixture of contact interlayers of transition metal salts. A low-cost metal electrode of molybdenum (Mo) with $\Phi$ = 4.5 eV is finely modulated between 4.2 eV and 4.9 eV by controlling the mixed concentration of the cesium carbonate ($Cs_2CO_3$) and vanadium pentoxide ($V_2O_5$) interlayer solution. The treated Mo electrodes are used as common source/drain electrodes in high-mobility ambipolar polymer semiconductor OFETs to determine the efficient injection properties for electrons and holes. The *n*- and *p*-channel device properties are also controllable by contact engineering, so that the complementary-like inverter based on the ambipolar semiconductor showed the best voltage-transfer behavior at the optimized mixed interlayer ratio.

## 2. Results and Discussion

**Figure 1** shows the structure of the top-gate/bottom-contact (TG/BC) OFET fabricated with the small band-gap polymeric and ambipolar semiconductor, diketopyrrolopyrrole-thieno[3,2-b]thiophene copolymer (DPPT-TT). OFETs using DPPT-TT, gold (Au) source/drain electrodes, poly(methyl methacrylate) (PMMA) dielectrics, and the same device structure have been reported to show high electron and hole mobilities of 1.56 and 1.36 $cm^2\ V^{-1}\ s^{-1}$, respectively.[27] The top-gated architecture incorporating hydroxyl-free polymer dielectrics, such as PMMA and CYTOP, has a number of advantageous features. For instance, the corresponding OFETs showed excellent ambipolar charge transport characteristics by means of minimizing extrinsic mobile charge traps at the hydroxyl groups at the semiconductor–dielectric interface and inducing efficient electron and hole injection from BC electrodes with a large injection area. Instead of Au, herein, we applied low-cost Mo as the BC metal for more practical use in cheap printed electronics. Although Mo is a promising alternative to Au in terms of its high electrical conductivity ($\approx 5 \times 10^{-6}\ \Omega$ cm) and low price (≈26 $/kg), its relatively low work function ($\Phi \approx -4.5$ eV) and easily formed native oxides can adversely influence charge-injection properties. In addition, the BC metal often shows a reduced $\Phi$ value due to hydrocarbons being adsorbed onto the surface, which results in push-back electron tails at the metal–semiconductor interface.[26]

To improve electron and hole injection, solution-processed $V_2O_5$ and $Cs_2CO_3$ interlayers were respectively deposited onto the bare Mo electrodes by a simple spin coating process. As

can be seen in the schematic diagram of Figure 1b, $V_2O_5$ and $Cs_2CO_3$ have different energy band structures. The electron affinity (EA) and ionization potential (IP) of the $V_2O_5$ films are reported to be 6.7 eV and 9.5 eV, respectively, and the Fermi level ($E_F$) is found to be nearly 0.3 eV below the conduction band minimum.[28] Notably, the as-received $V_2O_5$ is found to be natively *n*-doped; however, the EA and IP values sometimes showed 4.7–5.6 eV and 2.4 eV, respectively, due to its *p*-type nature after exposure to air.[28] The very high $\Phi$ of $V_2O_5$ generally induces an interface dipole and band bending due to the electrons transferred from organics to $V_2O_5$, and this results in *p*-doping to the organic semiconductor that is close to the metal–semiconductor interface.[28] Therefore, the $V_2O_5$ interlayer can be used as a hole-injection interlayer via increasing the $\Phi$ of the Mo electrode as well as *p*-doping the organic semiconductor in order to reduce the depletion width of the Schottky barrier at the contacts. In contrast, $Cs_2CO_3$ has a lower $E_F$ of ≈–3.3 eV and is typically regarded as an electron-injection material via inducing *n*-doping to the organic semiconductors and/or lowering the $\Phi$ of metal electrodes.[29–31]

With the aim of systematically controlling the injection properties and achieving enhanced electron and hole injection for better performance, we introduced a mixed interlayer system. A solution-processed metal salt-based interlayer for helping hole and electron injection ($V_2O_5$ and $Cs_2CO_3$) can be simply blended in a solution and then deposited by spin coating or spray printing onto metal electrodes. The $\Phi$ of Mo electrodes was measured by the Kelvin probe technique, from which the bare Mo has an $\Phi$ of –4.5 eV; meanwhile, different values of –4.9 eV and –4.2 eV are obtained for the purely $V_2O_5$- and $Cs_2CO_3$-treated Mo electrodes, respectively, as shown in **Figure 2**a. It is clear that the higher $\Phi$ of the Mo electrode with the $V_2O_5$ interlayer offers better hole injection, whereas the $Cs_2CO_3$ interlayer leads to improved electron injection by lowering the corresponding energy barrier for charge injection. Therefore, the ambipolar OFETs incorporating $V_2O_5$- and $Cs_2CO_3$-treated Mo electrodes can operate more predominantly in a *p*-channel and *n*-channel regime and show more balanced and/or more controllable ambipolar transport characteristics through the mixed interlayers [see Figure 1c].

Figure 2b–d shows the X-ray photoemission spectroscopy (XPS) measurement of the Mo electrodes treated by $V_2O_5$ and $Cs_2CO_3$ mixed interlayers. In Figure 2b, the Cs $3d_{3/2}$ and Cs $3d_{5/2}$ peaks of the $V_2O_5$:$Cs_2CO_3$ mixed interlayer films on Mo are situated at the binding energies of ≈739.1 eV and ≈725.1 eV, respectively. It needs to be noted that the intensities of the two

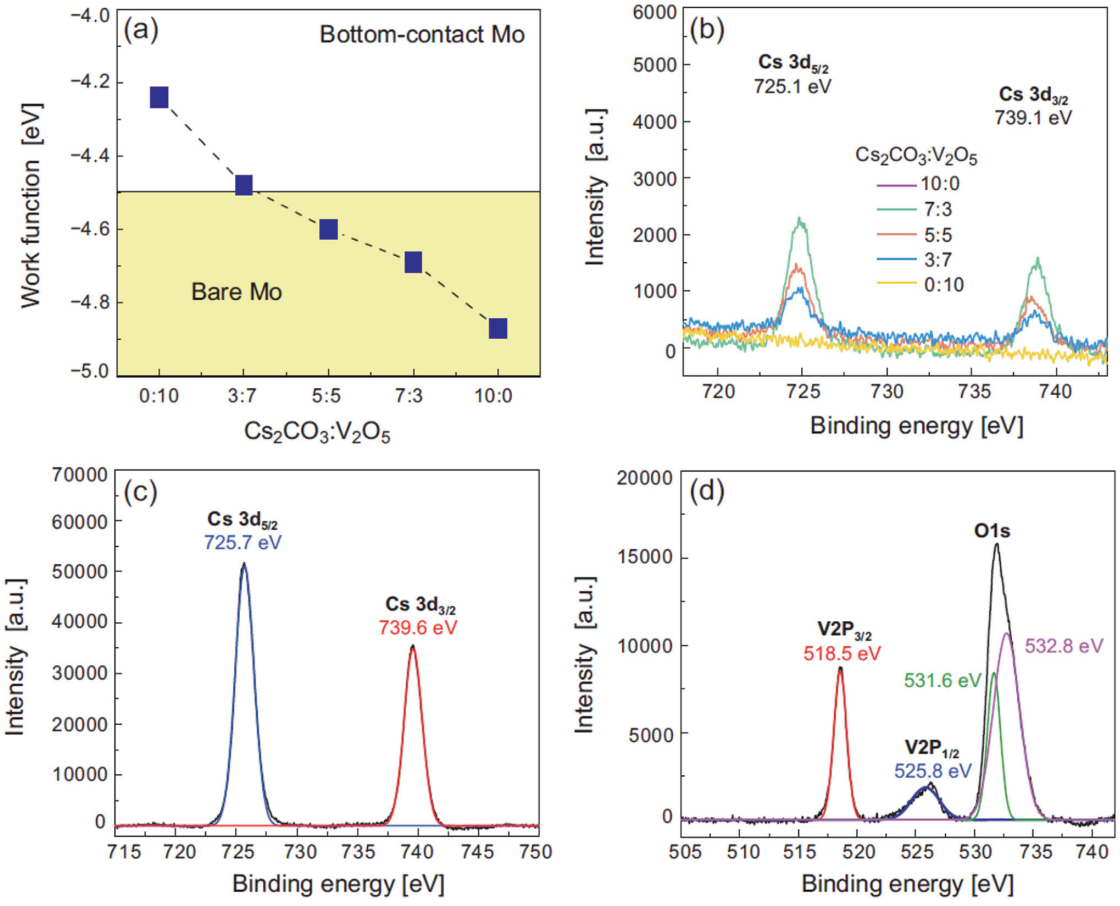


**Figure 2.** a) Work function of BC Mo electrodes with mixed interlayer at various blend ratios. b–d) X-ray photoemission spectra for $Cs_2CO_3$:$V_2O_5$ mixed interlayer-treated Mo electrodes; b) for a spin-coated film at various blend ratios and c,d) for a drop-casted film at 5:5 molar ratio between $Cs_2CO_3$ and $V_2O_5$.

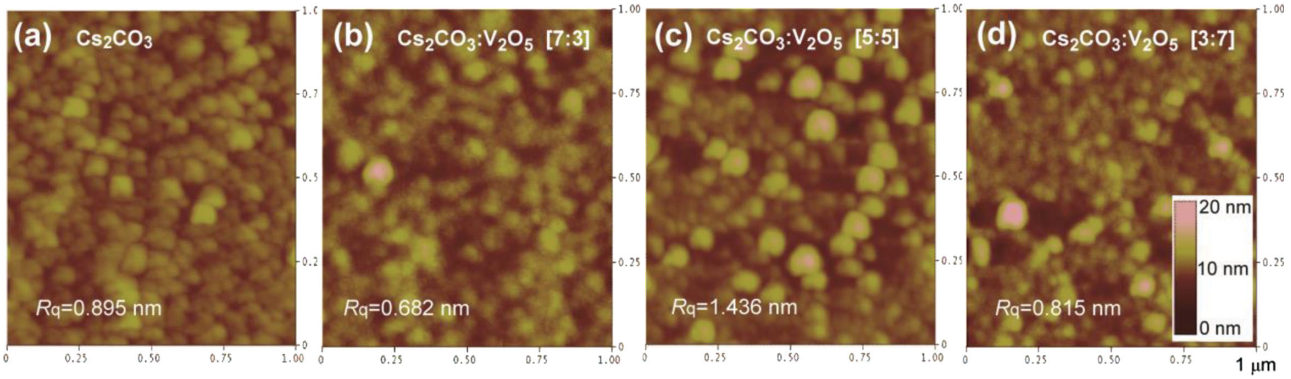


**Figure 3.** a–d) Tapping-mode AFM images of the a) pure $Cs_2CO_3$ film and $Cs_2CO_3$:$V_2O_5$ mixed interlayer films of b) 7:3, c) 5:5, and d) 3:7 molar ratios.

peaks are progressively decreased as the $Cs_2CO_3$ content is reduced from 100 to 70, 50, 30, and 0 molar percentages versus $V_2O_5$ content in a prepared blended solution before the film deposition by spin coating. In comparison with pure $Cs_2CO_3$ film, we could not find any distinctive peak shift of the binding energy for either Cs $3d_{3/2}$ or Cs $3d_{5/2}$ after blending with $V_2O_5$. This result indicates that intermixing $Cs_2CO_3$ and $V_2O_5$ neither causes chemical interactions nor changes their electronic structure, which can be altered by charge transfer (doping) in the mixed solid. In addition, we could not obtain the V $2p_{3/2}$ core level peaks in the XPS measurement for the same samples presumably due to the weak atomic sensitivity factor of the V 2*p* (1.95) as compared with Cs 3*d* (7.2) at a very small film thickness.[32] From a thick drop-casted interlayer film (Figure 2c,d), the V $2p_{3/2}$ and V $2p_{2/1}$ peaks appear at binding energies of ≈518.5 eV and ≈525.8 eV, respectively, which are associated with $V^{5+}$.[33] Moreover, O 1*s* core level peaks appear at binding energies of ≈531.6 eV and ≈532.8 eV, which corresponds to an oxygen atom in a 2- oxidation state in amorphous $V_2O_5$ and $Cs_2CO_3$ film, respectively.[33,34]

**Figure 3**a–d show tapping-mode atomic force microscope (AFM) images of pure $Cs_2CO_3$ [Figure 3a] and $Cs_2CO_3$:$V_2O_5$ mixed interlayer films on Mo electrodes with various molar ratios of 5:5, 3:7, and 7:3 [Figure 3c–d]. Although those solution-processed interlayers show submicrometer-sized aggregates and/or crystallites atop the Mo electrode, the overall electrode surface is fully covered by a ≈6–8 nm-thick thin film. The root-mean-square roughness ($R_q$) is in the range of 0.7–1.5 nm, which is slightly larger than that for a clean Mo surface (typically $R_q \approx 0.59$ nm). We believe that this slightly rough surface of the oxide interlayer film at the bottom of the organic semiconductor film does not significantly affect device performance, since in a top-gated OFET, most charge accumulation and charge transport occur at the semiconductor–dielectric interlayer, which is located at the top surface of the ≈30 nm-thick polymer semiconducting layer. As can be seen in **Figure 4**, the ambipolar DPPT-TT OFETs with mixed interlayer-treated Mo electrodes show relatively better transfer characteristics than devices with bare Mo electrodes (vide infra). The AFM images of spin-coated $Cs_2CO_3$:$V_2O_5$ mixed interlayer films also reveal no distinctive topological features or phase segregation in a multi-component system. When we measured XPS at various points in the samples, peak intensity was almost the same, which indicates the $V_2O_5$ and $Cs_2CO_3$ are uniformly distributed on the overall surface of the Mo electrode. The areal density of the two different components is merely controlled by changing the concentration of the metal salts in a blend solution.

Figure 4 shows the transfer characteristics [drain current ($I_d$) as a function of gate voltage ($V_g$)] of a group of DPPT-TT OFETs with various Mo electrodes. The DPPT-TT OFETs with bare Mo electrodes display typical ambipolar behaviors, manifesting as a V-shaped transfer curve with high hole and electron mobility of 1.5 (±0.2) $cm^2\ V^{-1}\ s^{-1}$ and 0.8 (±0.23) $cm^2\ V^{-1}\ s^{-1}$ at a drain voltage $V_d$ of –80 V and +80 V for *p*- and *n*-channel operation modes, respectively.[35] With respect to the bare-Mo-contacted devices, pure $V_2O_5$ and $Cs_2CO_3$ interlayers remarkably increase the OFETs' hole and electron mobility to 2.98 (±0.4) $cm^2\ V^{-1}\ s^{-1}$ and 2.6 (±0.41) $cm^2\ V^{-1}\ s^{-1}$, respectively, while the counter charge carriers' mobilities are inversely decreased to 0.4 (±0.15) $cm^2\ V^{-1}\ s^{-1}$ and 1.2 (±0. 3) $cm^2\ V^{-1}\ s^{-1}$. This implies that each interlayer played an important role in the improvement of ambipolar OFET performance by reducing the charge-injection barrier, but they take effect only selectively for either *p*-channel (via $V_2O_5$) or *n*-channel (via $Cs_2CO_3$) operation. Therefore, these two counter components can be intermixed and used to finely modify the ambipolar characteristics of OFETs. In Figure 4b–d (*p*-channel operation mode at $V_d = -60$ V and –80 V) and Figure 4e–g (*n*-channel operation mode at $V_d$ = +60 and +80 V), the drain current is considerably increased from 0.1 mA to 1 mA (for *p*-channel) and decreased from 0.27 mA to 0.075 mA (for *n*-channel), as the molar ratios of the $Cs_2CO_3$:$V_2O_5$ mixed interlayers are changed from 7:3, 5:5, and to 3:7. The corresponding hole mobility is found to progressively drop from 2.98 (±0.4) to 1.8 (±0.3), 1.4 (±0.4), 1.5 (±0.4), and 1.2 (±0.3) as the $V_2O_5$ concentration in the metal salt blend solution is decreased from 100 to 70, 50, 30, and 0 mol%, respectively. By contrast, the electron mobility is inversely increased from 0.4 (±0.15) to 1.1 (±0.36), 1.3 (±0.22), 1.8 (±0.38), and 2.6 (±0.41) $cm^2\ V^{-1}\ s^{-1}$, respectively, as the $Cs_2CO_3$ concentration is increased from 0 to 30, 50, 70, and 100 mol% in the mixed interlayer on the Mo electrodes. From these results, one can conclude that the *p*- and *n*-type properties of TG/BC ambipolar polymer transistors are mainly determined by the varied contact properties through controlling areal distribution and the surface coverage of $Cs_2CO_3$ and $V_2O_5$, and the two different transition metal oxides appear to play their roles

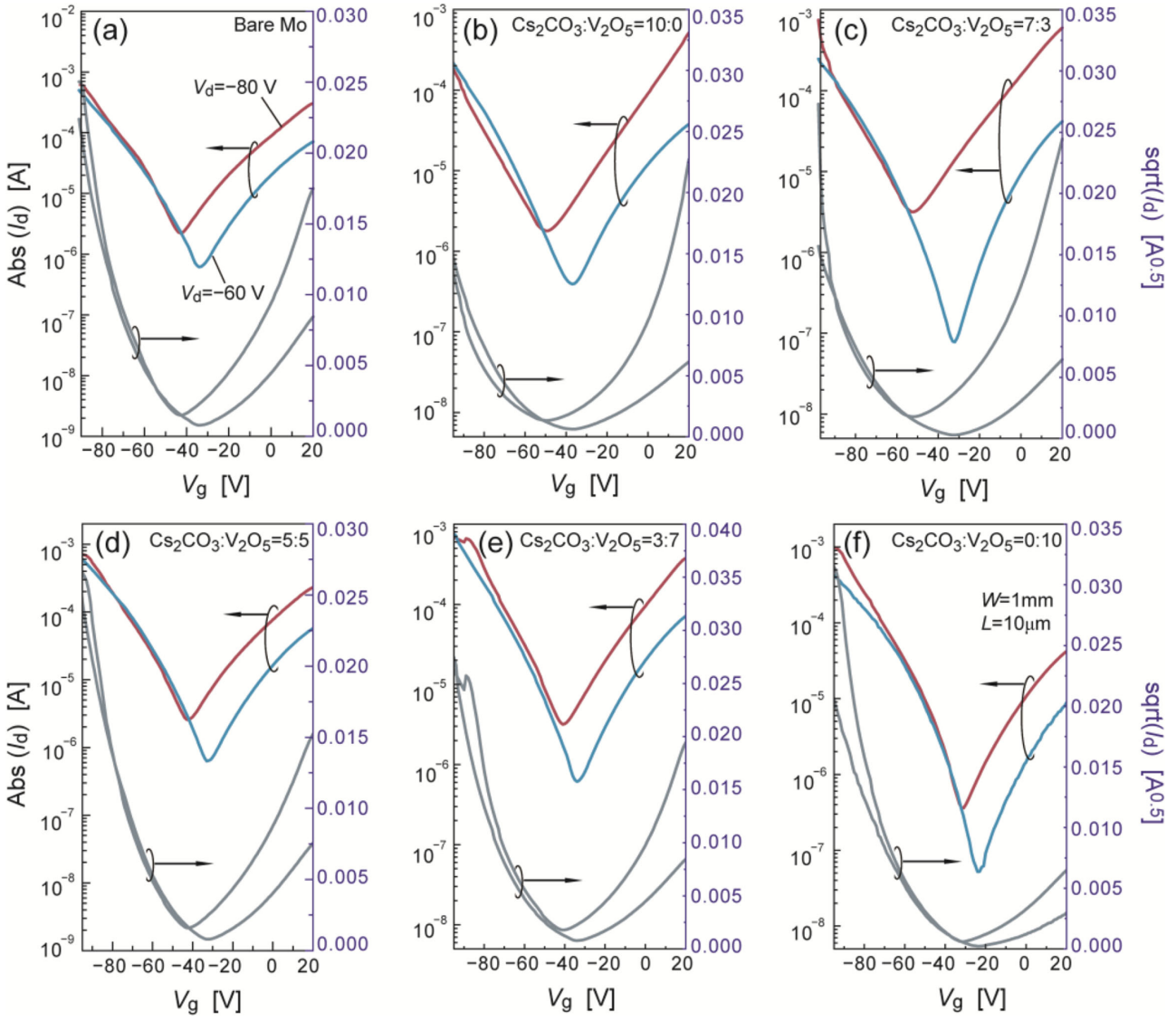


**Figure 4.** Transfer characteristics ($I_d$ vs $V_g$) of the DPPT-TT OFETs a–d) in *p*-channel regime (at $V_d$ = −60 V and −80V) and in *n*-channel regime (at $V_d$ = +60 V and +80 V), a,e) with bare Mo electrodes and $Cs_2CO_3$:$V_2O_5$ mixed interlayer-treated Mo electrodes of various blend ratios; b,f) 7:3, c,g) 5:5, and d,h) 3:7 molar ratios.

independently of each other, with no synergistic effect. It is interesting to observe that at the same concentration of $Cs_2CO_3$ and $V_2O_5$ (5:5 molar ratios), the resultant device performance is very similar to that for bare Mo electrodes.

The *p*- and *n*-channel OFET characteristics, which can be controlled by using various blend ratios of mixed interlayers, can be attributed to the modified charge-injection barrier between BC Mo electrodes and the highest occupied molecular orbital (HOMO = –5.33 eV relative to the vacuum level) and the lowest unoccupied molecular orbital (LUMO = –4.07 eV) of DPPT-TT, for the holes and the electrons, respectively. It is obvious that the purely $V_2O_5$-treated [or purely $Cs_2CO_3$-treated] Mo electrodes have the minimum barrier of ≈0.48 eV [or ≈0.2 eV] to hole [electron] injection, while counter charge carriers have the highest energy barrier of ≈1.06 eV for electrons [≈0.78 eV for holes] to be injected into the semiconductor. To further confirm the modulated charge injection, we analyzed the contact resistance. As shown in **Figure 5**b, the channel width ($W$)-normalized contact resistance ($R_c$) in the *p*-channel regime (for holes) of the OFETs with pure $V_2O_5$ treatment shows a value of ≈1.82 MΩ cm, which is smaller than that of the transistors with bare Mo and the Mo electrodes treated by pure $Cs_2CO_3$ and by other mixed interlayers. One needs to note that the $R_c$ is extracted by the Y-function method (YFM) for individual DPPT-TT OFETs [channel width/length ($W/L$) of 1 mm/20 μm].[36] Unlike the conventional transfer-length method (TLM), by which one can only obtain an average $R_c$ of the whole set of transistors having diverse channel lengths and the linear regression often suffers from error arising from parameter dispersion from transistor to transistor, the YFM offers a straightforward way to access the $R_c$ in a single transistor and thereby to access the evolution of the charge injection induced by different electrode materials.[36]

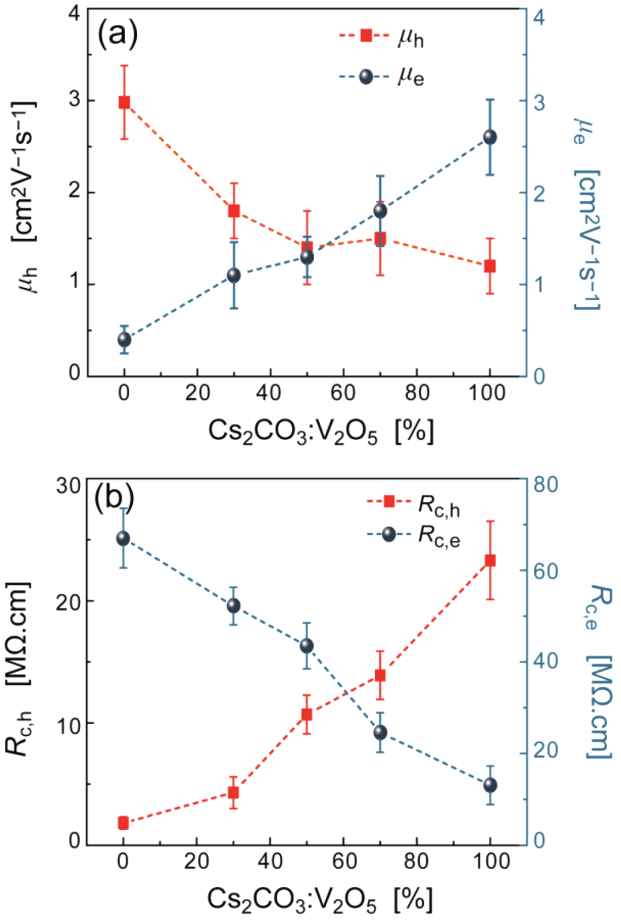


**Figure 5.** a) Hole- ($\mu_h$) and electron-mobility ($\mu_e$) of DPPT-TT OFETs at the saturation region ($V_d = \pm 80$ V) using Mo electrodes with $V_2O_5$:$Cs_2CO_3$ mixed interlayers at various molar concentrations of $Cs_2CO_3$ vs $V_2O_5$ from 0% to 30, 50, 70, and 100%. b) Contact resistance for *p*-channel regime ($R_{c,h}$) and *n*-channel regime ($R_{c,e}$) of the corresponding devices extracted by using the YFM.

In devices with mixed interlayers, the $R_cW$ for hole injection is constantly reduced from 13.9 MΩ cm to 7.6 MΩ cm and 4.3 MΩ cm as the $V_2O_5$ molar concentration is increased from 30 to 50 and 70 mol% versus the $Cs_2CO_3$, respectively. Therefore, the apparent hole and electron mobility and the corresponding overall ambipolar charge transport characteristics of the DPPT-TT OFETs are critically determined by the charge-injection behaviors through the mixed contact interlayer of $V_2O_5$ and $Cs_2CO_3$.

**Figure 6** shows the voltage-transfer characteristics (VTC, output voltage $V_{out}$ as a function of input voltage $V_{in}$) and corresponding gain of the inverters fabricated using ambipolar DPPT-TT OFETs with various interlayer configurations [at supplied bias ($V_{DD}$) of 80 V]. All inverters show typical Z-shaped VTC curves for ambipolar semiconductor devices. The bare Mo devices showed the $V_{in}$–$V_{out}$ voltage transfer at an inverting voltage ($V_{int}$) of ≈46 V with a gain of –40. The positive shift of $V_{int}$ from the ideal switching point at ½$V_{DD}$ is attributed to the larger saturation current of the pull-up transistor (*p*-channel operation) compared to that of the pull-down transistor (*n*-channel operation) due to the different electron and hole mobility and threshold voltage [see **Table 1**]. In Figure 6c, one can readily find a gradual shift in the $V_{int}$ from 50 V to 33.5 V as the $Cs_2CO_3$ molar concentration increases from 0% to 100% versus $V_2O_5$. This shift is due to the changing tendency for more favorable *n*-channel operation at higher concentration of electron injection component ($Cs_2CO_3$) in a mixed interlayer, thus the pulling down takes place at smaller $V_{in}$. Under optimized mixed interlayer conditions ($Cs_2CO_3$/$V_2O_5$ = 50% or 70%) achieving equivalent high mobility and low threshold voltage for both *p*-channel and *n*-channel transistors, the complementary-like inverter shows the best signal inverting characteristics; the $V_{int}$ is located near ½$V_{DD}$ and high gain as high as –80. Therefore, this contact engineering by varying the mixture constitution of oxide interlayer can enable better controllable CMOS-like circuits based on ambipolar OFETs.

## 3. Conclusions

In conclusion, we report on a mixed contact interlayer of two transition-metal oxides, $Cs_2CO_3$ and $V_2O_5$, for controlling the charge injection properties in ambipolar DPPT-TT organic transistors with using low-cost Mo source/drain electrodes. $Cs_2CO_3$ and $V_2O_5$ are found to greatly and independently enhance the charge injection for electrons and holes, respectively, by a large modulation of the Mo's work function [up to –4.2 eV (with $Cs_2CO_3$) and –4.8 eV (with $V_2O_5$)] and/or by introduction of *n*- or *p*-doping at the contacts. To realize concurrently the improvement of electron- and hole-injection and

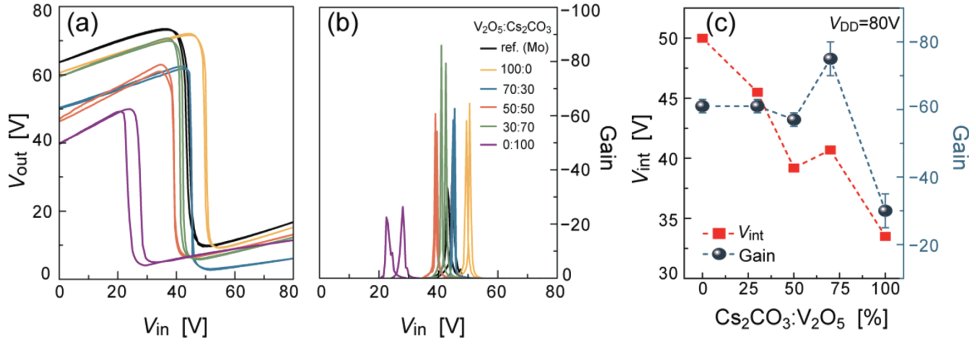


**Figure 6.** a) Voltage transfer characteristics and b) corresponding gain of the complementary-like inverter by using the DPPT-TT OFETs with different contact interlayer treatments [at $V_{DD}$ = 80 V]. c) The inverting voltage ($V_{int}$) and gain of the inverters at various interlayer concentration.

**Table 1.** Measured $\Phi$ values of Mo electrodes with pure or mixed interlayers, and electron ($\mu_e$) and hole mobilities ($\mu_h$), and $R_c$ of DPPT-TT OFETs using corresponding Mo electrodes in a *p*-channel regime (at $V_d$ = –80 V) and an *n*-channel regime (at $V_d$ = +80 V). Inverting voltage ($V_{int}$) and corresponding gain of complementary-like inverters at supplied bias ($V_{DD}$) of +80 V.

| $Cs_2CO_3$:$V_2O_5$ | $\Phi$ [eV] | *p*-channel OFETs (at $V_d$ = –80 V) | | *n*-channel OFETs (at $V_d$ = +80 V) | | Inverters (at $V_{DD}$ = +80 V) | |
|---|---|---|---|---|---|---|---|
| | | $\mu_h$ [$cm^2 V^{-1}s^{-1}$] | $R_{c,h}$ [MΩ cm] | $\mu_e$ [$cm^2 V^{-1}s^{-1}$] | $R_{c,e}$ [MΩ cm] | $V_{int}$ [V] | Gain |
| Bare Mo | –4.5 | 1.5 (±0.2) | 12.7 | 0.8 (±0.23) | 28.5 | 46 | –40 (±5) |
| 0:10 | –4.85 | 2.98 (±0.4) | 1.82 (±0.5) | 0.4 (±0.15) | 67 (±6.5) | 50 | –61 (±2) |
| 3:7 | –4.69 | 1.8 (±0.3) | 4.3 (±1.3) | 1.1 (±0.36) | 52.2 (±4.1) | 45.5 | –60 (±2) |
| 5:5 | –4.61 | 1.4 (±0.4) | 10.7 (±1.58) | 1.3 (±0.22) | 43.5 (±5) | 39.2 | –57 (±2) |
| 7:3 | –4.48 | 1.5 (±0.4) | 13.9 (±1.97) | 1.8 (±0.38) | 24.6 (±4.3) | 40.7 | –75 (±5) |
| 10:0 | –4.27 | 1.2 (±0.3) | 23.3 (±3.2) | 2.6 (±0.41) | 13.1 (±4.2) | 33.5 | –30 (±5) |

a systematic control of the apparent *p*- and *n*-channel ambipolar charge transport characteristics, $Cs_2CO_3$:$V_2O_5$ mixed interlayer at various molar ratios is attempted on the TG/BC DPPT-TT OFETs. Findings showed that the Mo's work function is very finely and constantly modulated between –4.2 eV and –4.8 eV by varying the molar ratio of the mixed interlayer. The high-performance DPPT-TT OFETs using such mixed interlayer-treated Mo source/drain electrodes exhibit great hole and electron mobilities as high as 2.98 and 2.6 $cm^2$ $V^{-1}$ $s^{-1}$, mainly due to the efficient charge injection promoted by the hole- and electron-injection interlayers of $V_2O_5$ and $Cs_2CO_3$. Moreover, the device properties for *p*- and *n*-channel operations are remarkably controllable by changing the composition of mixed interlayer film. All of the results proved that this contact engineering technique for ambipolar OFETs could be widely utilized in complementary-like organic circuits and other optoelectronic applications.

## 4. Experimental Section

*Field-Effect Transistor Fabrication*: TG/BC structure OFETs were fabricated on Corning Eagle 2000 glass substrate. After the conventional photolithography process of developing photoresist layer for source/drain electrode patterning, a 3 nm-thick Ti adhesion layer and a 20 nm-thick Mo contacting layer were deposited by sputtering the Ti and Mo targets and followed by the lift-off of photoresist. The substrates with patterned Mo/Ti electrodes were cleaned sequentially with an ultrasonic bath in deionized water, acetone, and isopropanol for 10 min each. The transition-metal oxides of $V_2O_5$ (adding small amount of $NH_3$ solvent) and $Cs_2CO_3$ were dissolved in 2-ethoxyethanol to obtain a concentration of 0.5 wt% solution. For the preparation of $V_2O_5$:$Cs_2CO_3$ mixed interlayer, each solution was blended at 7:3, 5:5 and 3:7 molar ratio, and then spin-coated onto the pre-cleaned substrates. An ambipolar polymer semiconductor of DPPT-TT was purchased from Luminescence Technology Corp. and used as received. The DPPT-TT was dissolved in anhydrous dichlorobenzene (DCB) to obtain a ≈10 mg/mL concentration solution, which was spin-coated on the bare Mo, or interlayer-treated Mo samples, and then annealed at 320 °C on a hot plate for ≈30 min in a nitrogen ($N_2$)-filled glove box. PMMA polymer dielectric was purchased from Sigma-Aldrich and used without further purification. The PMMA was dissolved in n-butyl acetate (nBA) at 80 mg/ml concentration and then spin-coated on the DPPT-TT layer followed by a thermal baking at 80 °C for ≈30 min in the same $N_2$-filled glove box to remove the residual solvents. The device fabrication was completed by deposition of aluminum (Al) as top-gate electrodes (≈50 nm thick) via thermal evaporation using metal shadow masks.

*Characterization*: The surface morphology of the thin film was investigated by tapping-mode AFM (NanoScope III, Veeco Instruments, Inc.) at the Korea Basic Science Institute (KBSI). X-ray photoemission spectroscopy (XPS) was measured using AXIS-NOVA (Kratos, Inc.) with a base pressure of $4.2 \times 10^{-9}$ Torr. The fundamental OFET electrical characterizations were carried out using a Keithley 4200 semiconductor characterization system in $N_2$-filled glove box.

## Acknowledgements

D.X.L. and K.-J.B. contributed equally to this work. This research was financially supported by the Pioneer Research Center Program through the National Research Foundation of Korea funded by the Ministry of Science, ICT & Future Planning (NRF-2013M3C1A3065528), LG Electronics, the National Research Foundation of Korea (NRF) grant funded by the Korea government (MSIP) (NRF-2014R1A2A2A01007159), the Dongguk University Research Fund of 2014, and the Primary Research Program of Korea Electrotechnology Research Institute (KERI).

Received: April 10, 2014
Revised: June 26, 2014
Published online: August 22, 2014

[1] A. Facchetti, *Chem. Mater.* **2011**, *23*, 733.
[2] H.-R. Tseng, H. Phan, C. Luo, M. Wang, L. A. Perez, S. N. Patel, L. Ying, E. J. Kramer, T.-Q. Nguyen, G. C. Bazan, A. J. Heeger, *Adv. Mater.* **2014**, 26, 2993.
[3] J. Li, Y. Zhao, H. S. Tan, Y. Guo, C.-A. Di, G. Yu, Y. Liu, M. Lin, S. H. Lim, Y. Zhou, H. Su, B. S. Ong, *Sci. Rep.* **2012**, *2*, 754.
[4] T. Sekitani, T. Someya, *Jpn. J. Appl. Phys.* **2012**, *51*, 100001.
[5] G. H. Gelinck, H. E. A. Huitema, E. van Veenendaal, E. Cantatore, L. Schrijnemakers, J. B. P. H. van der Putten, T. C. T. Geuns, M. Beenhakkers, J. B. Giesbers, B.-H. Huisman, E. J. Meijer, E. M. Benito, F. J. Touwslager, A. W. Marsman, B. J. E. van Rens, D. M. de Leeuw, *Nat. Mater.* **2004**, *3*, 106.
[6] T. Sekitani, H. Nakajima, H. Maeda, T. Fukushima, T. Aida, K. Hata, T. Someya, *Nat. Mater.* **2009**, *8*, 494.
[7] K. Jain, M. Klosner, M. Zemel, S. Raghunandan, *Proc. IEEE* **2005**, *93*, 1500.
[8] R. Søndergaard, M. Hösel, D. Angmo, T. T. Larsen-Olsen, F. C. Krebs, *Mater. Today* **2012**, *15*, 36.
[9] C. Pang, C. Lee, K. Y. Suh, *J. Appl. Polym. Sci.* **2013**, *130*, 1429.
[10] P. Heremans, G. H. Gelinck, R. Muller, K.-J. Baeg, D.-Y. Kim, Y.-Y. Noh, *Chem. Mater.* **2011**, *23*, 341.
[11] R. H. Kim, H. J. Kim, I. Bae, S. K. Hwang, D. B. Velusamy, S. M. Cho, K. Takaishi, T. Muto, D. Hashizume, M. Uchiyama,

P. André, F. Mathevet, B. Heinrich, T. Aoyama, D.-E. Kim, H. Lee, J.-C. Ribierre, C. Park, *Nat. Commun.* **2014**, *5*.
[12] E. van Veenendaal, G. H. Gelinck, J. Genoe, W. Dehaene, P. Heremans, in *Solid-State Circuits Conf. Digest Tech. Papers (ISSCC), 2011 IEEE Int.* St. Louis, MO **2011**, 322.
[13] R. R. Søndergaard, M. Hosel, F. C. Krebs, *J. Polym. Sci. Pol. Phys.* **2012**, *51*, 16.
[14] H. Klauk, *Chem. Soc. Rev.* **2010**, *39*, 2643.
[15] Q. D. Ling, D. J. Liaw, C. X. Zhu, D. S. H. Chan, E. T. Kang, K. G. Neoh, *Prog. Polym. Sci.* **2008**, *33*, 917.
[16] K.-J. Baeg, D. Khim, J. Kim, B.-D. Yang, M. Kang, S.-W. Jung, I.-K. You, D.-Y. Kim, Y.-Y. Noh, *Adv. Funct. Mater.* **2012**, *22*, 2915.
[17] K. J. Baeg, M. Binda, D. Natali, M. o. Caironi, Y. Y. Noh, *Adv. Mater.* **2013**, *25*, 4267.
[18] M. Muccini, *Nat. Mater.* **2006**, *5*, 605.
[19] K.-J. Baeg, M. Caironi, Y.-Y. Noh, *Adv. Mater.* **2013**, *25*, 4210.
[20] C. Liu, Z. Liu, H. T. Lemke, H. N. Tsao, R. C. G. Naber, Y. Li, K. Banger, K. Müllen, M. M. Nielsen, H. Sirringhaus, *Chem. Mater.* **2010**, *22*, 2120.
[21] Y.-Y. Liu, C.-L. Song, W.-J. Zeng, K.-G. Zhou, Z.-F. Shi, C.-B. Ma, F. Yang, H.-L. Zhang, X. Gong, *J. Am. Chem. Soc.* **2010**, *132*, 16349.
[22] Y. Zhang, C. Kim, J. Lin, T.-Q. Nguyen, *Adv. Funct. Mater.* **2012**, *22*, 97.
[23] E. J. Meijer, D. M. de Leeuw, S. Setayesh, E. van Veenendaal, B. H. Huisman, P. W. M. Blom, J. C. Hummelen, U. Scherf, T. M. Klapwijk, *Nat. Mater.* **2003**, *2*, 678.
[24] K. Szendrei, D. Jarzab, Z. Chen, A. Facchetti, M. A. Loi, *J. Mater. Chem.* **2010**, *20*, 1317.
[25] M. Treier, J.-B. Arlin, C. Ruzie, Y. H. Geerts, V. Lemaur, J. Cornil, P. Samori, *J. Mater. Chem.* **2012**, *22*, 9509.
[26] D. Natali, M. Caironi, *Adv. Mater.* **2012**, *24*, 1357.
[27] Z. Chen, M. J. Lee, R. Shahid Ashraf, Y. Gu, S. Albert-Seifried, M. Meedom Nielsen, B. Schroeder, T. D. Anthopoulos, M. Heeney, I. McCulloch, H. Sirringhaus, *Adv. Mater.* **2012**, *24*, 647.
[28] J. Meyer, K. Zilberberg, T. Riedl, A. Kahn, *J. Appl. Phys.* **2011**, *110*, 033710.
[29] F.-C. Chen, J.-L. Wu, S. S. Yang, K.-H. Hsieh, W.-C. Chen, *J. Appl. Phys.* **2008**, *103*, 103721.
[30] C.-I. Wu, C.-T. Lin, Y.-H. Chen, M.-H. Chen, Y.-J. Lu, C.-C. Wu, *Appl. Phys.Lett.* **2006**, *88*, 152104.
[31] K.-J. Baeg, J. Kim, D. Khim, M. Caironi, D.-Y. Kim, I.-K. You, J. R. Quinn, A. Facchetti, Y.-Y. Noh, *ACS Appl. Mater. Interfaces* **2011**, *3*, 3205.
[32] D. Briggs, M. P. Seah, *Practical Surface Analysis, Auger and X-ray Photoelectron Spectroscopy*, Vol. *1*, John Wiley and Sons, Chichester, UK **1990**.
[33] A. Benayad, H. Martinez, A. Gies, B. Pecquenard, A. Levasseur, D. Gonbeau, *J. Electron Spectrosc. Relat. Phenom.* **2006**, *150*, 1.
[34] J. Huang, Z. Xu, Y. Yang, *Adv. Funct. Mater.* **2007**, *17*, 1966.
[35] S. M. Sze, K. K. Ng, *Physics of Semiconductor Devices*, Wiely Interscience, New Jersey **2007**.
[36] Y. Xu, T. Minari, K. Tsukagoshi, J. A. Chroboczek, G. Ghibaudo, *J. Appl. Phys.* **2010**, *107*, 114507.